Chapter VI: Structure and Magnetic Properties of TiO_2 Thin Films Deposited by e-Beam Evaporation

In the previous chapter, we have demonstrated ferromagnetism in both TiO_2 as well as Co-doped TiO_2 thin films deposited by PLD technique. Though ferromagnetism in TiO_2 has been reported by few groups, still there is no report on the magnetic properties of TiO_2 thin films deposited by e-beam evaporation technique. To establish the universality of ferromagnetism in nanostructured TiO_2 thin films, this chapter is solely dedicated to explore the magnetic properties of TiO_2 thin films grown on Si substrate by e-beam evaporation technique. After deposition, the films are annealed under constant flow of high purity O_2 and Ar gas at 500 ^oC in a tubular furnace for 1h separately and then slowly cooled down to room temperature. The pristine film (deposited on Si/quartz), annealed in oxygen and argon are referred as film P, A and B, respectively. In addition, we have also deposited thin films from Co (2 at %) doped TiO_2 target.

6.1 Structural Properties

Fig.6.1 shows the oxygen resonance RBS data of the pristine thin film deposited on Si substrate using a piece from the Co (2 at %) doped TiO_2 sintered target as used in the PLD technique (discussed in Chapter V). The thickness of the film has been kept 100 nm with the help of a quartz crystal thickness monitor. The Co, Ti, Si and O edges are quite prominent in the spectrum. The peak corresponding to Co shows a combination of three peaks in the RBS plot. It suggests non-uniform distribution of Co throughout the film. Comparing the areas corresponding to Co and Ti, it is clear that the atomic concentration of the former is higher than the latter. It suggests faster evaporation of Co than Ti. Hence, e-beam evaporation technique is not suitable for deposition of Co-doped TiO_2 thin films. So, we have not further studied these films and have focused only on the TiO_2 films. Fig.6.2 depicts the GAXRD pattern of the films P, A and B. Film P does not show any peak in the diffraction pattern and indicate its amorphous nature. When annealed in Ar and O_2 atmosphere, diffraction peaks observed at 25.3^o, 37.9^o and 48.1^o for the

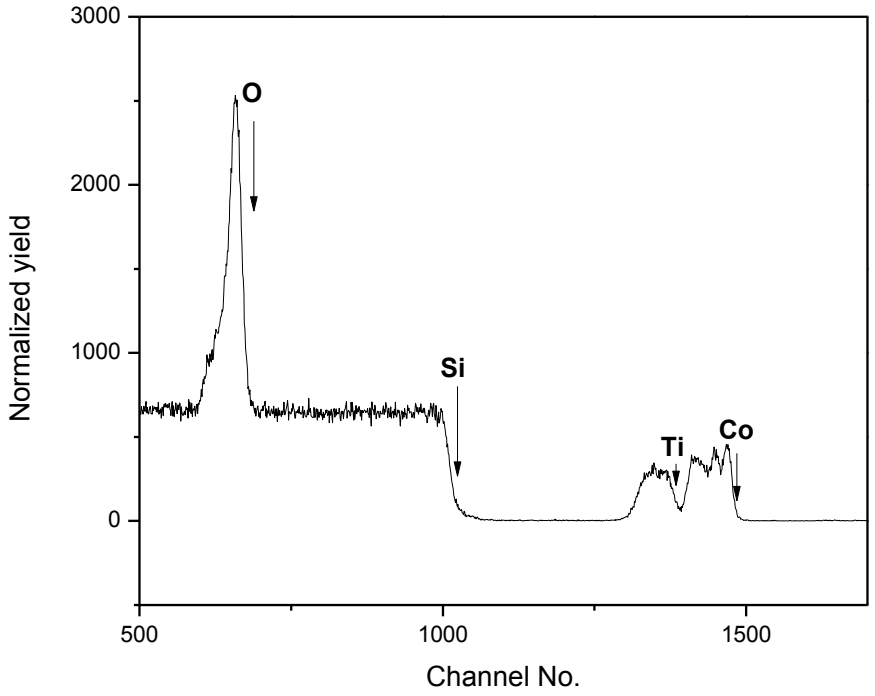

Fig.6.1 Oxygen resonance RBS data of the pristine thin film deposited on Si substrate from Co-doped TiO_2 target.

film A and B corresponding to the planes (101), (004) and (200) of anatase phase of TiO_2 (ICDD Card No.89 - 4921). No peak related to any impurity phase has been observed. While sharp (101) peak in film A indicates higher degree of crystallinity, more broadening in XRD peak in case of film B suggests smaller crystallite size. The average crystallite size calculated using Scherrer equation is found to be ~ 19 nm and ~ 7 nm for the film A and B, respectively. To explore surface morphology of these films, we have carried out FE-SEM and SPM measurements.

FE-SEM micrographs of both film A and B are shown in Fig. 6.3. From the micrographs, it is revealed that in some particular regions, particles are agglomerated indicating non-uniform deposition of the particle flux on the

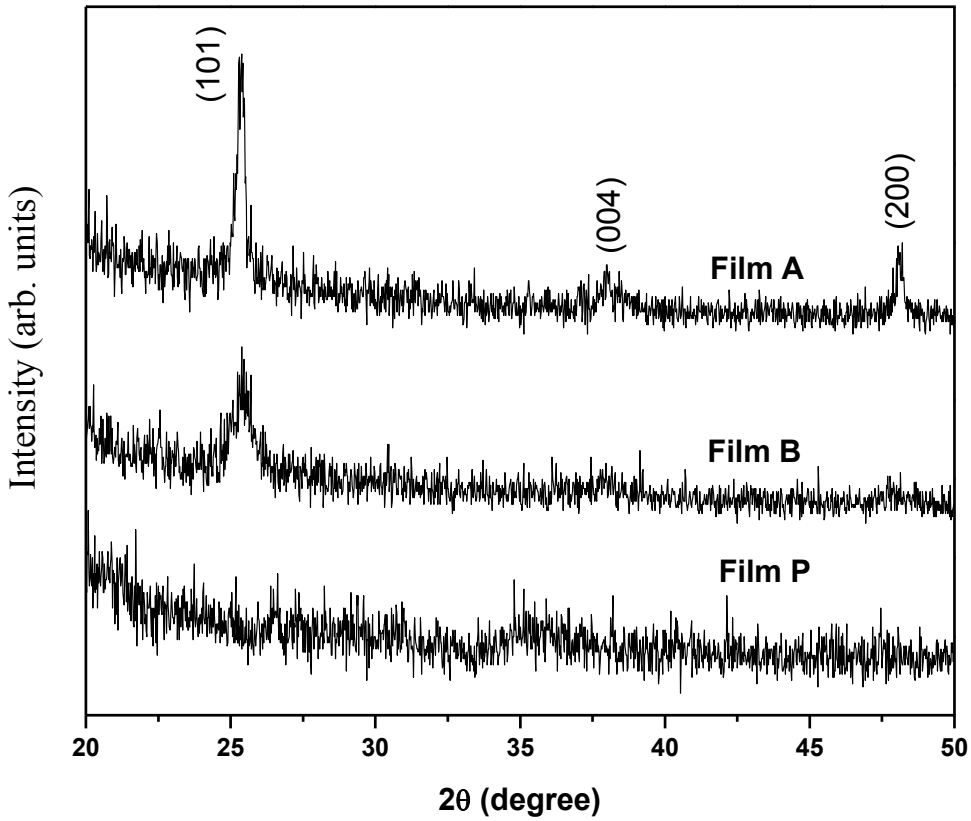

Fig.6.2 GAXRD pattern of TiO_2 thin films deposited on Si substrate (film P), annealed in O_2 (film A) and Ar (film B) atmosphere.

substrate (Fig.6.3). However, the surfaces are found to be crack free. A typical energy dispersive x-ray spectroscopy (EDS) spectrum is shown as the inset of Fig.6.3 (b) indicating the presence of Ti and O only.

Fig.6.4 (a) and (c) depict the surface topography of film A and B, respectively. The scan surfaces are equal to 5 εm x 5εm in area. Topography of the films indicate uniform along with smooth surface. Fig.6.4 (b) and (d) represents the 3D view of the surface topography of the films A and B, respectively. From the 3D representation, one may note that the film B is having nano-hillock like structures distributed randomly over the film surface. The surface roughness has been quantitatively expressed by the root-mean-

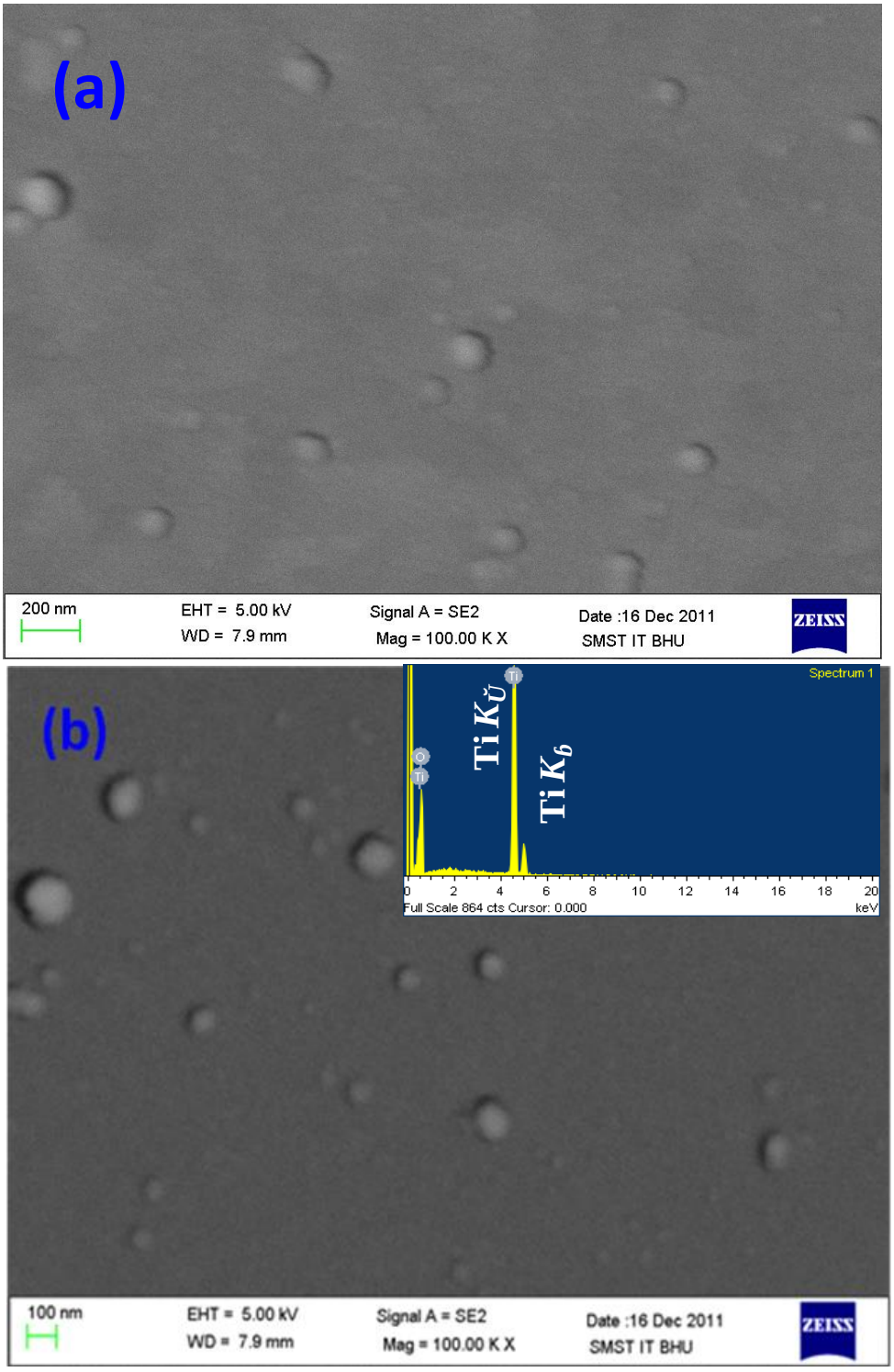

Fig.6.3 FE-SEM micrograph of TiO_2 thin film annealed in (a) O_2 (film A) and (b) Ar (film B) atmosphere @ 500 ^oC. Inset of (b) represents a typical EDS spectrum of the film measured at 20 kV.

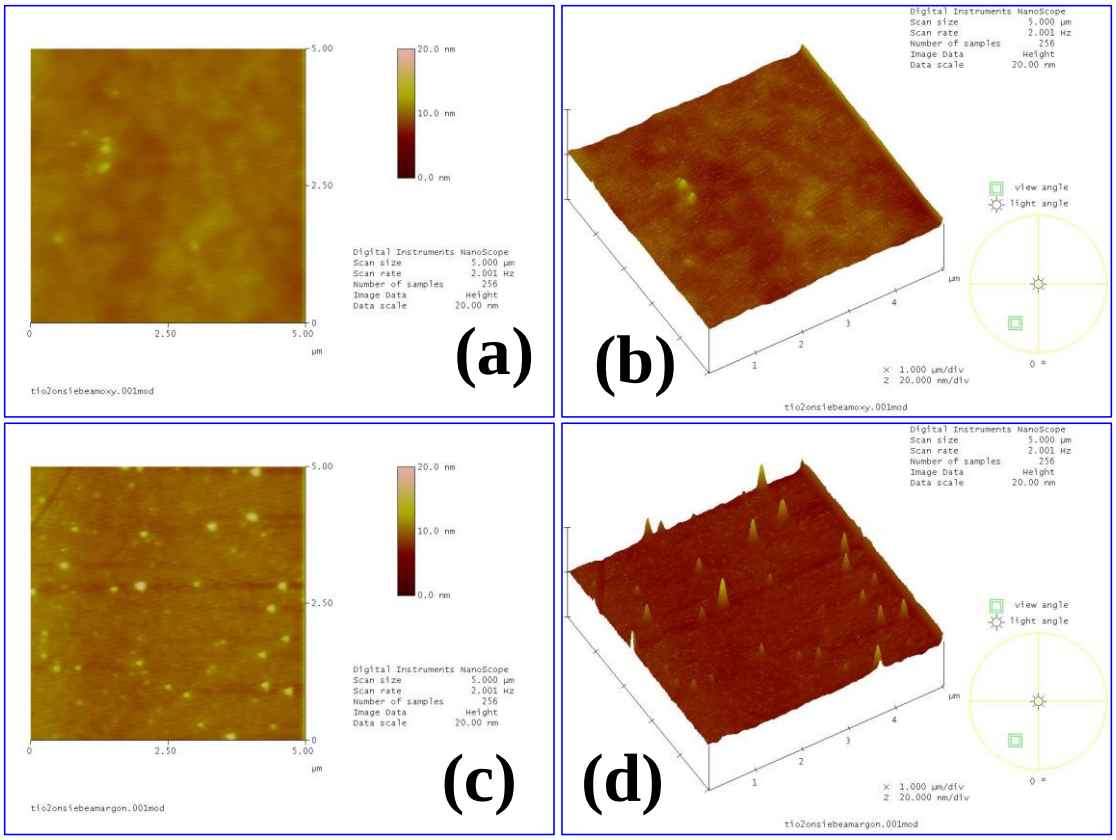

Fig.6.4 SPM images of TiO_2 thin film deposited on Si and annealed in (a) O_2 (film A) and (c) Ar (film B) atmosphere. (b) and (d) represents the 3D view of the film A and B, respectively.

squared roughness (R_{rms}) which is defined as the root means square average of height deviation taken from the mean data. It is expressed as:

$$\tilde{a}\ \text{Æ}\ z_i^2/n = R_{rms} \qquad (6.1)$$

Where z_i is height at i^{th} position of the tip and n is the number of data points [User's Manual Veeco Instruments]. Nanoscope IV controller (version 5.30r1, 2004) software has been employed for the measurement of the above parameter. The roughness (R_{rms}) calculated for the film A and B yields ~ 0.5 nm and ~ 0.8 nm respectively, indicating the latter film is having higher roughness than the former one. Though the phase is anatase in both the films and same thickness, surface roughness is quite different for O_2 and Ar annealed films.

Further, we have carried out the optical studies of films P, A and B which are deposited on quartz substrates in the same run and are annealed under similar conditions. The optical transmission of the film is shown in Fig.6.5. The oscillations observed in the transmission spectra represent the interference of the transmitted light from the different atomic planes of the film and substrate [Swanepoel (1983)]. These oscillations are the fingerprint of the good quality film as evidenced from the FE-SEM and SPM results. The appearance of the crest and trough at nearly same wavelength in the transmission spectra indicates similar thickness of the films. In the parabolic band structure approximation, the band gap E_g and the absorption coefficient ñŬò of an indirect band gap semiconductor are related through the well-known equation:

$$Ŭhз = A\,(hз - E_g)^2 \quad é\ é\ é\ é\ é\ é\ é\ é\ é \quad ..(6.2)$$

Where ñAò is a constant of proportionality, Ăħ is Planck's constant and ñзò is the frequency of incident photon [Smith (1978)]. In the present case, the band gap (E_g) of the films is calculated by plotting $(Ŭhз)^{1/2}$ as a function of incident photon energy (hз) and linearly regressing the linear portion of the $(Ŭhз)^{1/2}$ to zero of the energy axis. By this method, E_g is found to be 3.47 for the film P and A, and 3.43 eV for the film B (inset of Fig.6.5). The higher band gap observed for the film P is possibly due the fine particles that compose the film which is also evident from the GAXRD results. From the transmittance spectra of the films, the refractive index (n) and porosity (P) are calculated using the modified envelope method [Swanepoel (1983)]. Refractive index and porosity measured at wavelength of 530 nm is found to be almost same for all the films i.e. 1.4 and 81.4, respectively. One may note that, except the surface roughness and crystallinity, all other parameters are quite similar in both the film A as well as film B. To further check the thickness of the films and possible contaminations, we have carried out RBS measurements.

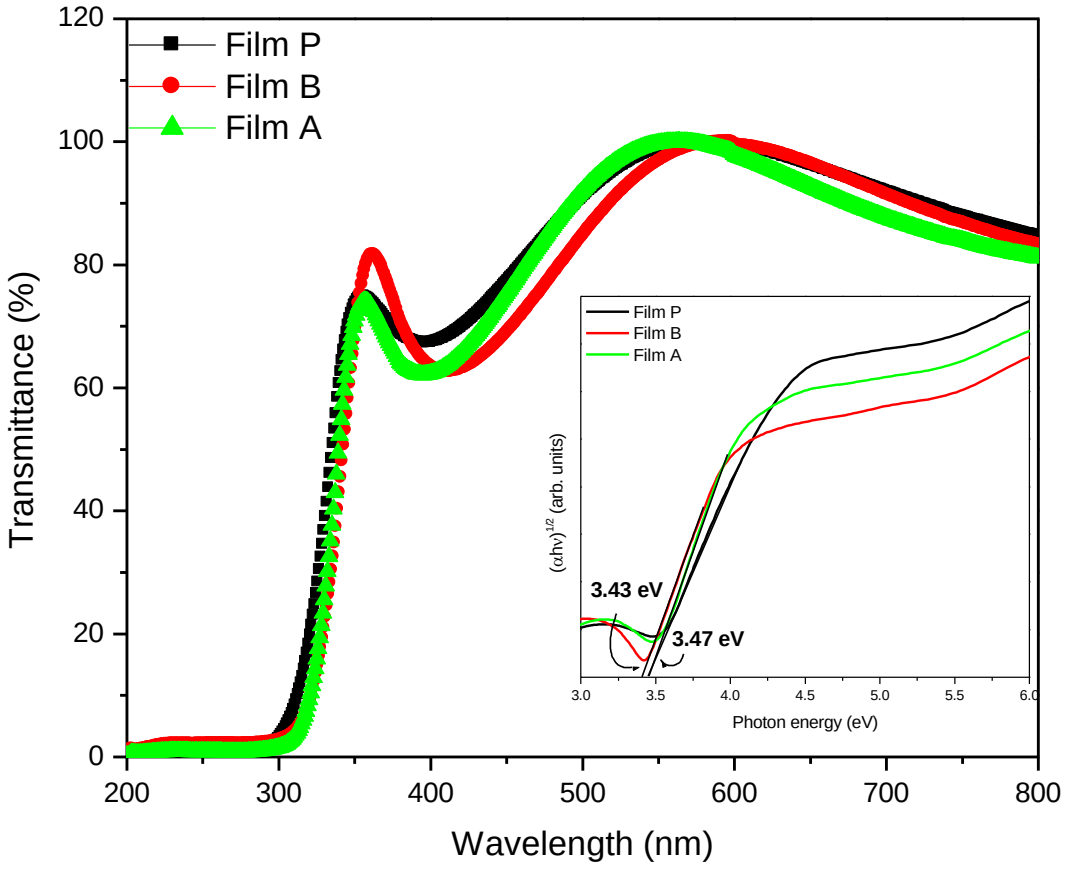

Fig.6.5 Transmittance as a function of incident wavelength (ə). The inset shows the $(\check{U}h\text{з})^{1/2}$ as a function of incident photon energy (hз).

Fig.6.6 depicts the RBS data of film A and B, respectively. Besides Ti, Si and O, no other element has been detected from the RBS measurements. The symmetrical shape of the peaks corresponding to the elements Ti and O indicate their uniform distribution throughout the film. Also, the width of the spectrum related to Ti is almost same for both the films indicating the films are having same thickness.

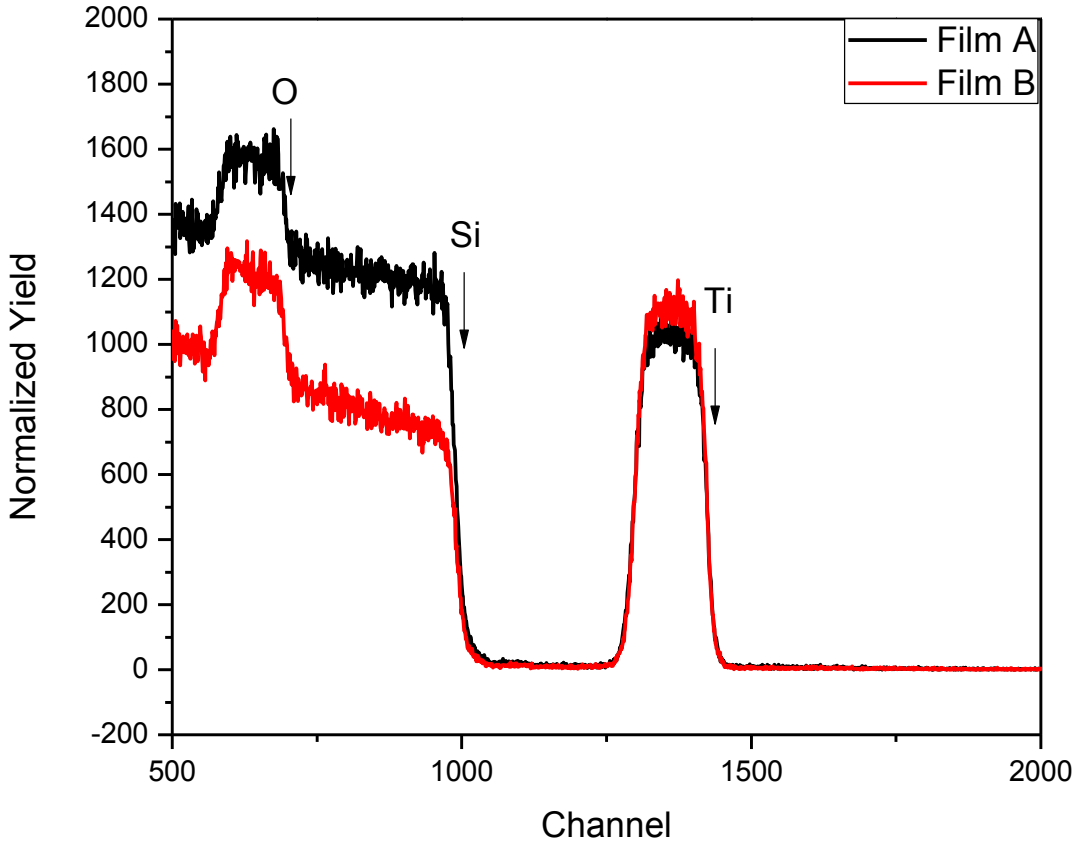

Fig.6.6 RBS data of the film A and B indicating Ti, Si and O edges.

6.2 Magnetic Properties

The magnetic measurements of the films are carried out by using a SQUID-VSM (from Quantum Design, USA). Si substrate and TiO_2 ingot used for film deposition are found to be non-magnetic. Further, we have checked the contamination during the handling process by keeping a Si substrate inside the deposition chamber with subsequent evacuation without any deposition. Then the substrate has been taken out of the chamber and kept under O_2 flow for 1h at 500 ÁC in a tubular furnace. The *M* vs. *H* measurement of the Si substrate undergone the handling process is shown as Fig.6.7.

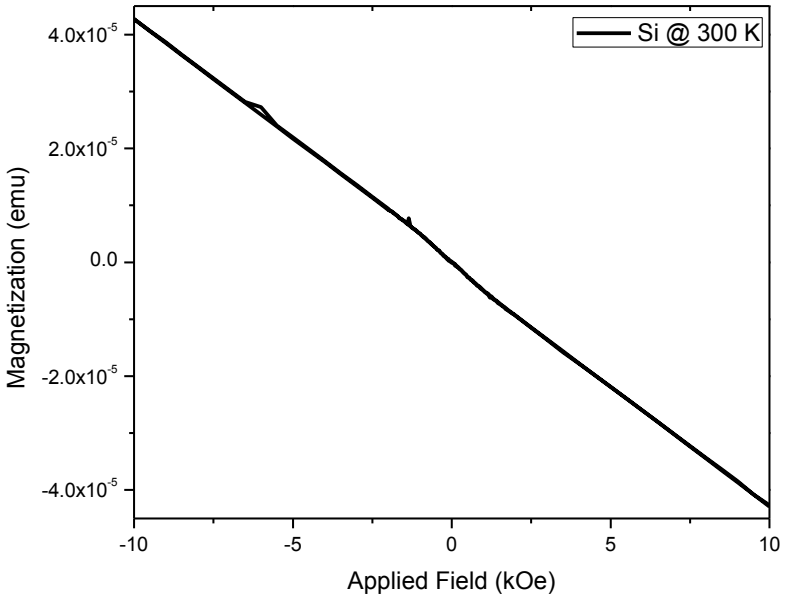

Fig.6.7 Magnetisation as a function of applied magnetic field for the Si substrate.

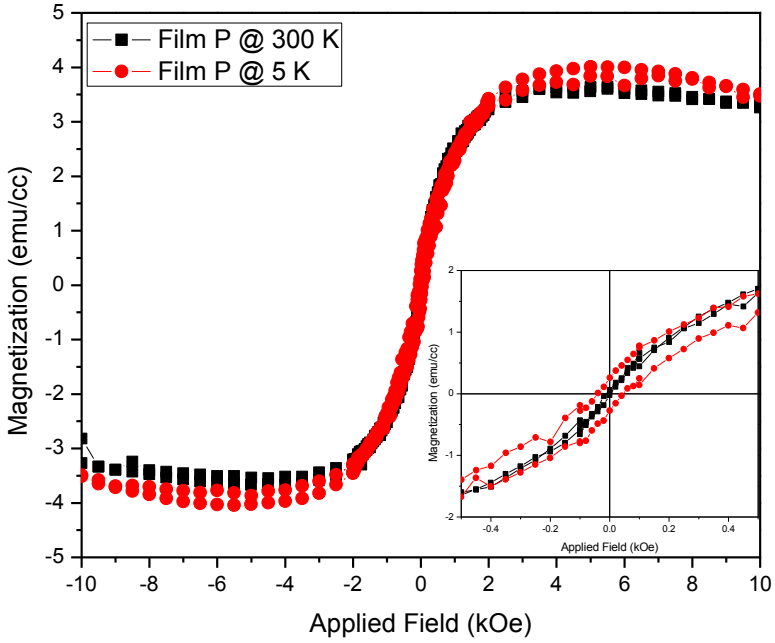

Fig.6.8 Magnetisation as a function of applied magnetic field for the film P at 300 and 5 K (inset shows the zoomed view of the *M-H* loop at low fields).

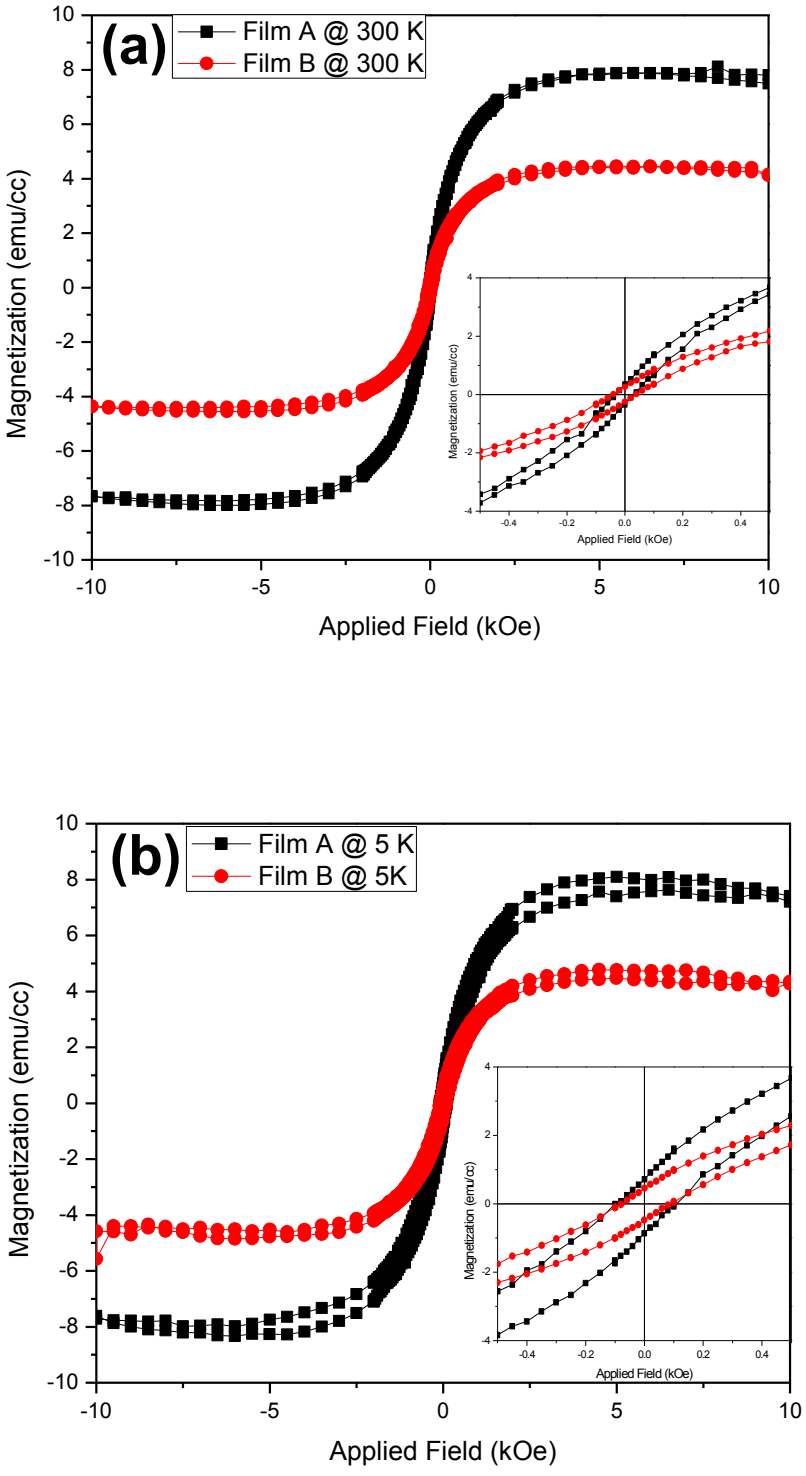

Fig.6.9 Magnetisation as a function of applied magnetic field for the film A and B at (a) 300 and 5 K (b) (insets show the zoomed view of the *M-H* loops at low fields).

The *M* vs. *H* behaviour clearly indicates the diamagnetic nature of the substrate that clearly refutes the possible contamination during the course of handling. Magnetisation as a function of applied magnetic field measured at 300 and 5 K for the film P is depicted in Fig. 6.8. The diamagnetic contribution from the Si substrate has been subtracted from the *M* vs. *H* data [Venkatesan et al. (2004)]. In case of film P measured at 300 K, magnetisation saturates at low field (2.5 kOe) and after reversing the field in negative direction, magnetisation is retraced along the same path. Zero coercivity and remanence observed from the *M-H* plot suggests the super-paramagnetic behaviour in case of film P. However, at 5 K slight opening of the hysteresis loop has been observed with coercivity ~44 Oe and remanence 0.26 emu/cc. It indicates the superparamagnetic blocking temperature (T_B) lie in between 5 and 300 K.

The *M* vs. *H* plots for the film A as well as B measured at 300 and 5 K are shown in Fig.6.9. Magnetisation increases with increase in applied magnetic field and almost saturates at 10 kOe applied field. Both films A and B demonstrate hysteresis, indicating ferromagnetism at 300 K. At 300 K, the coercivity is found to be 31 Oe and 42 Oe, whereas remanence obtained is 0.36 emu/cc and 0.26 emu/cc for the films A and B, respectively (shown as inset of Fig.6.9 (a)). *M* vs. *H* at 5 K, shows increase in the values of coercivity to 102 Oe and 80 Oe with subsequent increase in remanence to 0.72 and 0.45 emu/cc for the film A and B, respectively (shown as inset of Fig.6.9(b)). Here, we would like to point out that the film annealed in O_2, shows higher saturation magnetisation (M_s) than that of the Ar annealed film measured at 300 K as well as at 5 K. This observation is in sharp contrast with earlier works where higher magnetisation is found in films annealed in inert/vacuum atmosphere reported by Sudakar et al. (2008). Chang et al. (2012) shows disappearance of ferromagnetism in oxygen annealed SnO_2 film. The saturation magnetisation (M_s) is found to be 7.9 emu/cc for the film A and 4.4 emu/cc for the film B measured at 300 K which are significantly higher than the earlier reports. For example, magnetisation measured at 10 kOe field for anatase TiO_2 film

deposited by sol-gel on alumina substrate is found to be 2 emu/cc [Kim et al. (2009)]. We have shown magnetisation of ~3 emu/cc for the same film deposited on Si substrate by PLD technique [Mohanty et al. (2012)]. It is reported that the magnetisation is found to be greatly influenced by the thickness of the film. Magnetisation decreases gradually with increase in film thickness due to negligible contribution from oxygen vacancies [Sudakar et al. (2008), Chang et al. (2012)]. It seems that the magnitude of the magnetic moment greatly depends on the deposition technique, substrate and thickness of the films. However, in the present case, the higher saturation magnetisation obtained in case of film A compared to film B may not be explained on the basis of above criterion as both of them are deposited by the same technique, deposited on same substrate [Si: n-type (100)] and are having same thickness as well.

6.3 Discussion

There are other undoped oxides like HfO_2, In_2O_3, SnO_2 and ZnO without any transition metal doping show room temperature ferromagnetism. One of the well accepted reason behind room temperature ferromagnetism in undoped transition metal oxide is defects like oxygen vacancies. To have ferromagnetism, presence of unpaired d electrons is necessary. However, ferromagnetism observed in the aforementioned semiconducting materials having no *d* electrons is often termed as d^o magnetism [Coey et al. (2005), Hong et al. (2006), Yoon et al. (2006), Venkatesan et al. (2004)]. In the previous chapter, we have shown that TiO_2 films deposited by PLD technique at various oxygen partial pressures are ferromagnetic at room temperature [Mohanty et al. (2012)]. Basically, the oxygen vacancies are considered to be the n-type dopant in TiO_2 that might be the reason for the magnetic order. Besides thin film, we have also demonstrated higher magnetic moment in TiO_2 than Co-doped TiO_2 nanoparticles, solely due to oxygen vacancies as discussed in detail in Chapter IV [Mohanty et al. (2011)].

Fig.6.10 (a) demonstrates the XPS survey scans for the film A and B which looks identical and does not display the presence of any foreign elements. To investigate further, the O 1*s* and Ti 2*p* core levels have been scanned. Fig.6.10 (b) and its inset, depicts the oxygen 1*s* core level spectra with asymmetry around the binding energy ~ 530 eV in both films as well as bulk TiO_2, respectively. So, the spectra have been fitted with two Gaussian peaks with Shirley background, denoted as Oa and Ob respectively, using XPS peak4.1 software package [from http:/www.uksaf.org/software.html]. The Oa peak is attributed to the oxygen atoms of TiO_2 [Kallel et al (2009)]. The Ob peak is assigned to the hydroxyl groups, chemisorbed oxygen and organic oxygen contamination on the surface of the film [Bessergenev et al. (2006)]. Comparing the area ratio of Oa to Ob, it is clear that film A has relatively higher oxygen vacancies on the film surface compared to the film B [Naeem et al. (2006)], which might be the cause of higher magnetic moment in the former. At the same time, in bulk TiO_2 we have found a negligible area under Ob peak (inset of Fig.6.10 (b)) indicating minimum oxygen vacancies which is predictable. Hence, we can say that in thin films, the surface oxygen vacancies are higher than the bulk. Sharma et al have suggested another evidence of increase in oxygen vacancies with shift in O 1*s* peak position towards higher binding energy [Sharma et al. (2011)]. Fig.6.10 (b) clearly indicates a shift of 0.3 eV in O 1*s* core level position towards the higher binding energy for the film A. Therefore, comparison of area ratio of Oa to Ob as well as shifting in O 1*s* core level peak confirms the higher oxygen vacancies in film A than in B. This argument is also supported from the slight higher absorbance observed in case of film A than film B in the visible wavelength region (Fig.6.5). Fig.6.10 (c) illustrates the Ti 2*p* core level spectra. However, we do not observe the presence of Ti^{3+} and Ti^{2+} by deconvoluting the Ti $2p_{3/2}$ core level spectra. Ti $2p_{3/2}$ core level has been fitted well with single peak as shown in Fig.6.10 (c). The difference in the binding energy of Ti $2p_{1/2}$ and $2p_{3/2}$ core levels i.e. 5.8 eV confirms the Ti^{4+} valence state in both the films. A careful observation

indicates a shifting in Ti 2*p* level towards lower binding energy in case film A compared to film B (Fig. 6.10 (c)). Sharma et al. (2011) have shown that Ti 2*p* core level shifts towards lower binding energy as an indication of creation of more oxygen vacancies which is in good agreement with our results. We have examined the interfacial defects or impurities contributing to the magnetism in TiO_2 thin film. To do so, we have performed a cross-sectional TEM of the representative film A (Fig.6.11). The distinct lattice fringes as observed in Fig.6.11 confirm the crystalline nature of the film. EDS of the substrate taken at various locations does not show any contamination (a typical EDS pattern of Si substrate is shown as inset). No impurity has been observed from careful examination of the sample by cross-sectional TEM. Therefore, we have confirmed that RTFM in the present case is due to the oxygen vacancies rather than creation of Ti^{3+}/Ti^{2+}. Similar to our results, Rumaiz et al. (2007) attribute the magnetism to oxygen vacancies instead of Ti^{3+}/Ti^{2+}cation formation.

The presence of an oxygen vacancy is associated with two electrons which may localize onto the neighboring Ti ions transforming it into Ti^{3+} or may be delocalized in the TiO_2 matrix. The other possibility could be one of the two electrons be delocalized in the TiO_2 matrix and the other will be localized onto Ti ions transforming them into Ti^{3+}. However, Wei et al. (2009) have explained that the oxygen 2*p* electron plays an important role in the exchange interaction and ferromagnetic ordering. The large overlap between neighboring oxygen 2*p* orbital ensures an effective interaction range and relatively high ordering temperature, in spite of low net magnetic moment [Wei et al. (2009)].

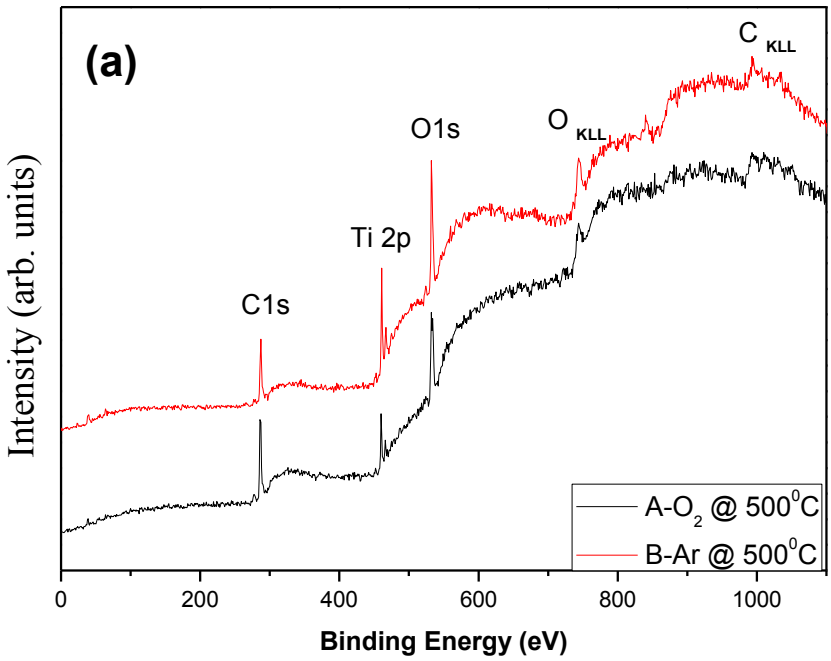
(a)
C KLL
O1s
O KLL
Ti 2p
C1s
Intensity (arb. units)
A-O2 @ 500°C
B-Ar @ 500°C
0
200
400
600
800
1000
Binding Energy (eV)

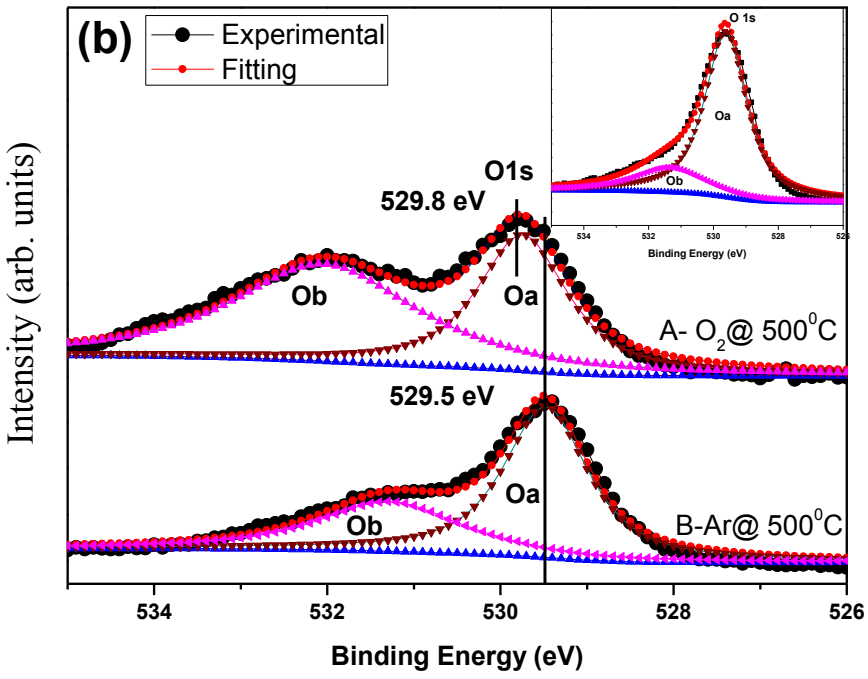
(b)
Experimental
Fitting
O1s
529.8 eV
Ob
Oa
A- O2@ 500°C
529.5 eV
Oa
Ob
B-Ar@ 500°C
Intensity (arb. units)
534
532
530
528
526
Binding Energy (eV)
O 1s
Oa
Ob
Binding Energy (eV)

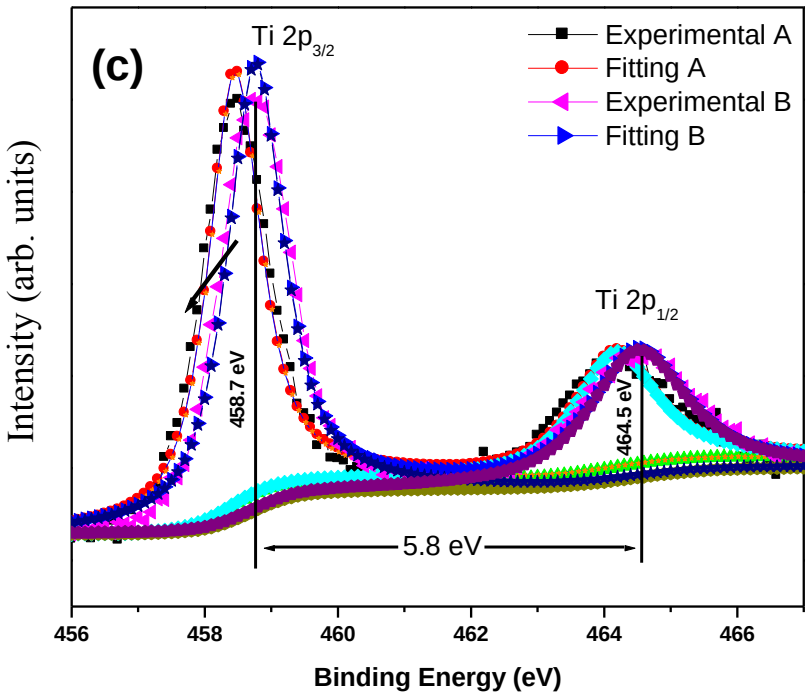

Fig.6.10 (a) XPS survey scan of TiO_2 films annealed in O_2 and Ar (b) Oxygen 1*s* core level spectra of the films: Inset shows the O 1*s* core level spectra for bulk TiO_2 with Gaussian fitting with Shirley background (c) Ti 2*p* core level spectra of the films.

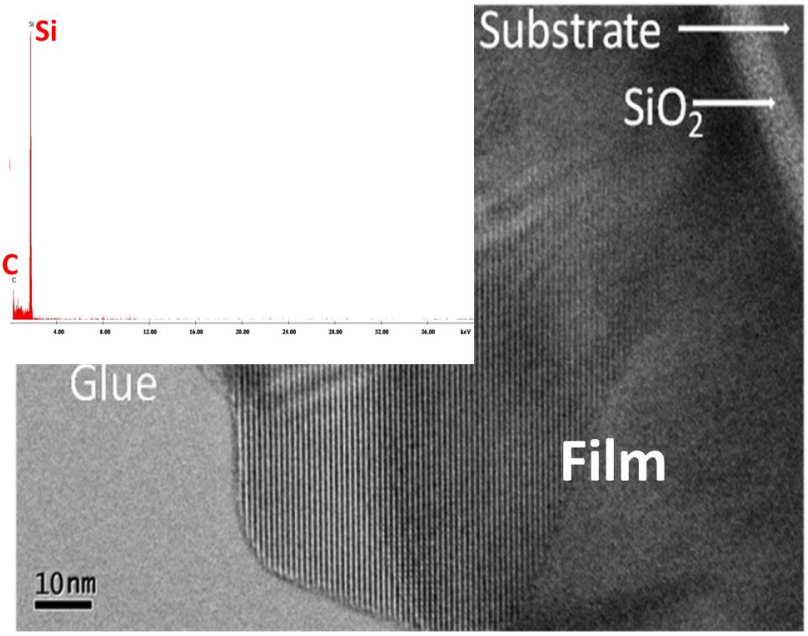

Fig.6.11 High resolution cross-sectional transmission electron micrograph of the TiO_2 film on Si substrate. The inset shows the EDS of the Si substrate (x-axis from 0 - 40 keV).

Sundaresan and Rao (2009) have concluded that the electrons trapped in oxygen vacancies (F Centers) are possibly polarized and give rise to RTFM. Kim et al. (2009) have observed RTFM in both anatase and rutile phases of TiO_2. The higher magnetic moment observed in rutile has been attributed to more oxygen defects in the distorted TiO_6 octahedra [Kim et al. (2009)]. Crystallinity has also been found to play a vital role in deciding the extent of magnetisation in the films [Mohanty et al. (2012)]. As discussed in Chapter V, we have already shown that highly crystalline Co-doped TiO_2 film deposited by PLD at 0.1 mTorr oxygen partial pressure shows high degree of magnetisation (8 emu/cc) which is about four times than the film deposited at 1 mTorr [Mohanty et al. (2012)]. Therefore, the observation of RTFM with high magnetic moment in oxygen annealed film as in the present case could be the result of complex interplay of oxygen vacancies, crystallinity and surface roughness. Hence, ferromagnetism observed in TiO_2 thin films deposited by e-beam evaporation technique, confirm the defect induced magnetism in nanostructured TiO_2 thin films irrespective of the deposition or growth condition. We propose a mechanism for the observed ferromagnetism in TiO_2.

MECHANISM

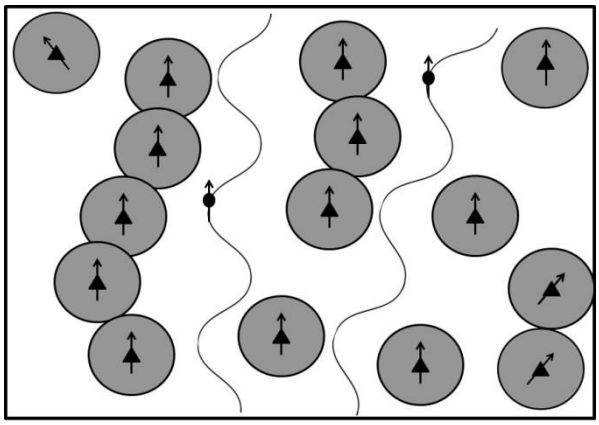

Fig. 6.12 Schematic representation of magnetic polarons in TiO_2. The solid triangles represent the oxygen vacancies where an electron, shown as an arrow is localized. The grey circles represent the electron wave-function. The delocalized electrons are denoted as an arrow on a dark circle.

In TiO_2, as oxygen vacancy is associated with two electrons, it may be localized at the oxygen vacancy site or may be delocalized in the matrix as

itinerant electrons. The localized carriers at the oxygen vacancy sites form bound magnetic polarons (BMP) (Fig.6.12). A polaron is basically a correlated state of an electron and lattice vibration. In Fig.6.12, the solid triangles represent the oxygen vacancies where an electron, shown as an arrow, is localized within the grey circle representing a BMP (Fig.6.12). The overlapping of these BMPs polarizes the magnetic moment in that cluster. The grey circles represent the electron wave-function. The other mechanism that explains the ferromagnetism is Ruderman- Kittel-Kasuya-Yosida (RKKY) model. In RKKY picture, the long range ferromagnetic order is established through the movement of delocalized electrons in the matrix (Fig.6.12). In TiO_2, the carrier binding energy is less and has been estimated in the range of ~ 4 - 41 meV by different authors [Calderon and Sarma (2007)]. When the thermal energy exceeds the carrier binding energy, a fraction of electrons are promoted (i.e., thermally activated) as delocalized electrons. Now the exchange interaction of the spin of the delocalized electron and the polarized cluster of BMPs leads to a long range ferromagnetic ordering. So in TiO_2, competition of both RKKY and BMP model leads to the observed ferromagnetism and conduction in these systems.

6.4 Summary

- Pristine TiO_2 thin films deposited by electron beam evaporation technique show superparamagnetic behaviour and after annealing in either O_2 or Ar atmosphere demonstrate ferromagnetism at room temperature.
- X-ray photo emission spectroscopy (XPS), Raman spectroscopy, Rutherford's backscattering spectroscopy (RBS), cross-sectional transmission electron microscopy (TEM) and energy dispersive x-ray spectroscopy (EDS) refute the possible role of impurities/contaminants exhibiting ferromagnetism at room temperature in these films.
- Higher saturation magnetisation of O_2 annealed film than the Ar annealed one, further demonstrate higher crystallinity which also possess uniform deposition as well as smoother surface in comparison to the latter one.
- The observed magnetism in TiO_2 is ascribed to the competing effect of RKKY and BMP models